Long-range and high-resolution traffic monitoring based on pulse-compression DAS and advanced vehicle tracking and classification algorithm

Iñigo Corera ⬤, Enrique Piñeiro ⬤, Javier Navallas ⬤, Mikel Sagues ⬤ and Alayn Loayssa ⬤

Institute of Smart Cities and Department of Electrical, Electronic and Communications Engineering, Universidad Pública de Navarra, 31006 Pamplona, Spain

* Correspondence: alayn.loayssa@unavarra.es

Abstract: We demonstrate traffic monitoring over tens of kilometres of road using an enhanced distributed acoustic sensing system based on optical pulse compression and a novel transformed-domain-based processing scheme with enhanced vehicle detection and tracking capabilities. EXTENDER

1. Introduction

Automatic traffic monitoring schemes have attracted great interest in the past years due to the the growing demand for actionable information for the effective management of transport networks. AÑADIR ALGUNA REFERENCIA A OTROS SISTEMAS DE MONITORIZACIÓN DE TRÁFICO

Distributed Acoustic Sensing (DAS) is a fiber optic sensor technology that has received considerable attention in later years due to its wide range of applications in a variety of fields such as structural health monitoring [1], pipeline monitoring [2], seismic sensing [3], intrusion detection [4] or railway traffic monitoring [5]. Besides, DAS sensors are now starting to be considered in the field of roadway traffic monitoring, as they provide some unique capabilities, linked to their distributed nature, when compared to other technologies as loop detectors, magnetic sensors, radar sensors, microwave detectors or even video cameras [6–9].

Roadway traffic monitoring requires of high sensitivity and long-distance sensing capabilities, which, in principle, could be achieved using several DAS setups [10]. For instance, direct-detection phase-sensitive optical time-domain reflectometry sensors, which are based on detecting changes in the amplitude of the backscattered signal from a particular position in the fiber as a result of excitations, have demonstrated long-range measurement capability [4,11]. However, these sensors present a highly nonlinear response to excitation that makes it difficult to quantify the actual vibration in the fiber. Other schemes are based on optical coherent-detection, using a local oscillator to demodulate the full optical field (amplitude and phase) so that the changes in the optical path length between close locations in the fiber can be determined by subtracting the phase of the backscattered signal from those locations [12]. This differential-phase coherent optical time-domain reflectometry (COTDR) setups have an intrinsic advantage for long-range applications because the measured backscattered signal is proportional to the amplitude of the optical field instead of its power.

The DAS sensor type that has the best capability to provide the longest possible range measurements in a purely passive link without additional distributed amplification

is based on a refinement of the differential-phase COTDR setup in which optical pulse compression (OPC) is implemented [13,14]. OPC is based on the same principles that have been applied for decades in radar systems but translated to the optical domain [15,16]. In OPC, waveforms with long duration (high energy) and high time-bandwidth product are launched into the fiber so that the back-reflected signals can be processed upon reception with matched filters to produce narrow effective pulse widths. Therefore, OPC greatly relaxes the trade-off between spatial resolution and range in COTDR DAS sensors providing an enhancement in the measurement signal-to-noise ratio (SNR) that naturally leads to long-range measurements. The SNR improvement brought by OPC is, in principle, proportional to the increased duration (energy) of the compression waveform compared to the use of a simple pulse. However, OPC performance is constrained by the phase noise of the laser source [15,17,18]. We have recently studied this effect in detail developing a theoretical model and finding that the sensitivity of OPC-COTDR degrades due to phase noise as the pulse duration is increased [19]. Furthermore, we have demonstrated a technique to compensate for the effects of the phase noise of the laser source so that OPC-OTDR can be applied in long-range measurements using lasers with less stringent phase noise requirements [OFS22].

In this work, we introduce a traffic monitoring scheme deploying, for the first time to our knowledge, optical pulse compression (OPC) implemented in a coherent optical time-domain reflectometry (COTDR) setup [19]. We also introduce a new vehicle detection and tracking algorithm based on a novel transformed domain, in which each point corresponds to a specific straight segment that can be related to vehicle trajectories in the non-transformed domain.

The technique has been experimentally tested by performing live measurements along a 40-km telecommunication fiber cable running in a buried microduct pipe along a road opened to traffic. Experimental results show that each type of vehicle (cars, trucks, motorbykes...) has a different "DAS footprint", allowing us to classify them using machine learning algorithms. A supervised learning model based on support-vector machines (SVM) has been used for the classification stage within Matlab Classification Learner App, where the evaluation was performed under a five-fold cross-validation scheme with 80% of the observations dedicated to training and 20% of the observations dedicated to test. Excellent results were obtained, with a classification rate of 98.8% for vehicle passing events, a 99.8% for car passing events and a 88.8% for trucks.

2. Installation of the fiber and sensor configuration

The experiments were performed on a spare dark fiber on a 40-km telecommunication fiber cable which is currently used by Gobierno de Navarra to connect two of its premises. The cable is installed buried in the shoulder of a two-way road inside a microduct pipe using the conventional air blowing method. Vehicles circulating on the road generate small vibrations on the pavement which propagate through the ground, reaching the optical fibers inside the cable. These vibrations are detected by the DAS sensor, so that a signal processing scheme can be implemented to detect and track the vehicle. All the measurements shown in this paper were performed simultaneously over the entire length of the fiber, but the specific data highlighted in the figures correspond to the one-kilometre section of the road that is shown in Figure 1. This location was selected because a video camera could be used to monitor the whole road section and provide an independent verification for the vehicle detection and tracking provided by our sensor.

Distributed acoustic measurements were carried out using a sensor prototype, implementing the coherent OTDR configuration shown in Figure 2. In this setup, the output of a narrow linewidth laser source is split into two branches. One branch is directly connected to the local oscillator input of a homodyne receiver that comprises a 90° dual-polarization optical hybrid and four balanced detectors, so that polarization diversity is provided. The other branch is fed to a Mach-Zehnder electrooptic modulator (MZ-EOM) that in the experiments is used to translate to the optical domain the linear frequency modulated (LFM)
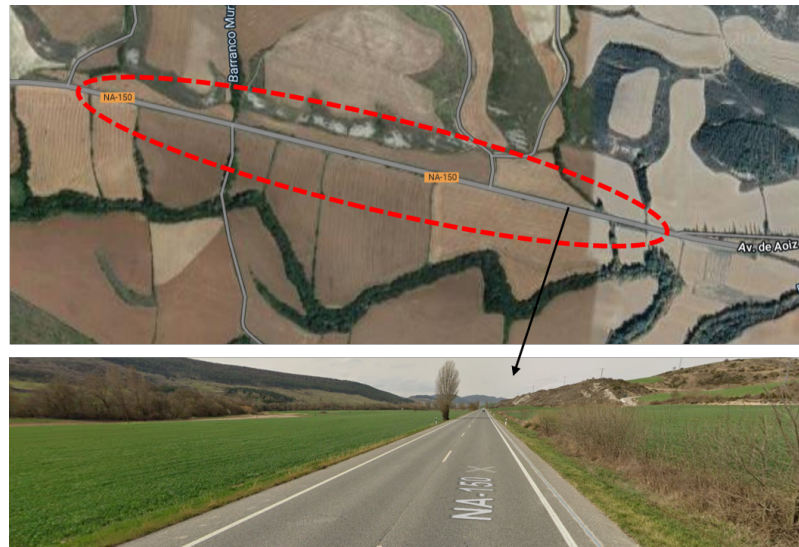
**Figure 1.** Section of the telecommunications cable link.

pulses, that are generated by an arbitrary waveform generator (AWG). The MZ-EOM is biased at minimum transmission so that it generates optical double-sideband supressed-carrier (ODSB-SC) modulation. LFM pulses with 4-μs duration and 50-MHz peak-to-peak frequency deviation centered at 50-MHz are used in these measurements. Therefore, in the optical domain 2 simultaneous LFM pulses (one at each side of the optical carrier) are obtained. The resulting spatial resolution after matched filtering in reception is 2-m. The output of the MZ-EOM is amplified in an EDFA and launched into the sensing fiber. Finally, the backscattered signal from the fiber is detected in the homodyne receiver and then digitized and post processed in a computer. The pulse repetition frequency was set to 200 Hz, as this was found to be enough to carry out the subsequent signal processing required to detect and track vehicles.

A first preprocessing stage is applied to the raw DAS recording in order to combine the information of the different pulsed sidebands, which experience different Rayleigh scattering statistics, to compensate fading. This stage is based on the application of the rotated-vector-sum method [20], with a previous spatial moving averaging with a length of 6 m, a summation of the optical field vectors corresponding to the different sidebands, the extraction of the phase from the resultant optical field vector and the computation of the phase difference between samples separated by a gauge length of 6 m so that enough granularity was provided for accurate detection of individual vehicles. Then, the phase data is band pass filtered from 0.3 to 3.5 Hz, where the fundamental quasi-static components that are dominant in traffic seismic signals are concentrated. After applying this signal preprocessing steps, high sensitivity and resolution signals are obtained, which are then fed to the vehicle detection and tracking algorithm.

3. Automatic traffic detection and tracking

Figure 3 (a) depicts a heat-map displaying the differential phase detected by the DAS sensor along different times (vertical axis) and locations (horizontal axis) corresponding to the 1-km section of the two-way road in Figure 2 (a). The aim of the system is to provide, from this preprocessed DAS recording, the trajectories of the vehicles passing through the monitored road; i.e., automatically identify the vehicles and provide their spatial position along the road as a function of time. To achieve this goal, the traffic detection and tracking algorithm is divided into two steps: local segment detection and segment tracking.

When considering a short time interval, we can assume that vehicles are moving at a constant velocity, implying a locally linear segment signature in the DAS recording. Therefore, the recording is divided in processing blocks corresponding to short time intervals, so that straight segments corresponding to moving vehicles are to be detected at each of
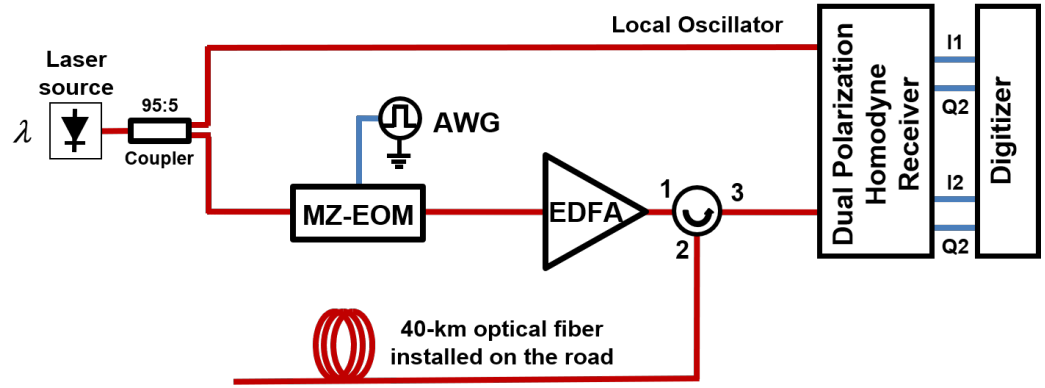
Figure 2. Experimental setup.
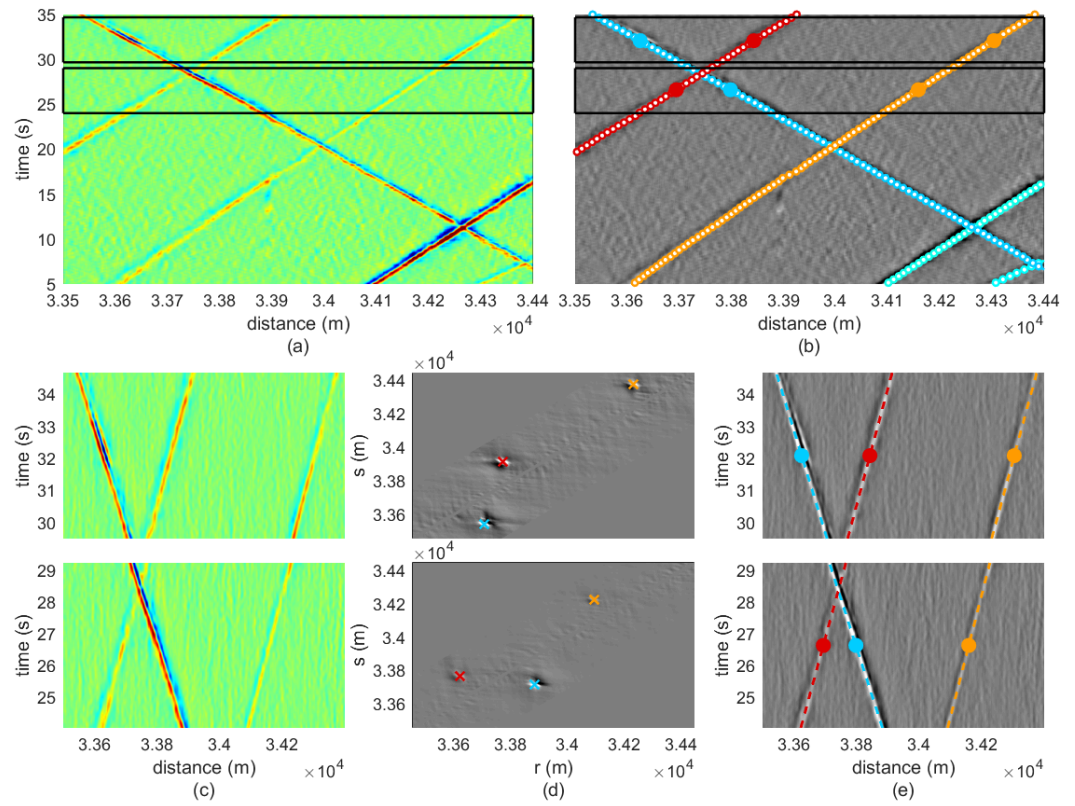
Figure 3. (**a**) Measured vibration intensity and (**b**) results of the vehicle detection and tracking algorithm. (**c**) Detail of the measured vibration intensity (**d**) transformed-domain and (**e**) resulting segments after segmentation, for the two time-distance blocks marked with black square boxes in (**a**).

these blocks. Specifically, the processing blocks comprise a time span, Δt, of 5 s. Blocks are calculated every $\delta t = 0.35$ s, so that the temporal overlapping between consecutive blocks is 4.65 s. Two non-consecutive blocks are marked with black square boxes in Figure 3 (a) and shown with more detail in Figure 3 (c).

The segment detection algorithm applied at each block relies on a newly proposed transformed domain, in which each point corresponds to a specific straight segment in the normal non-transformed recording domain. Detecting vehicle segments corresponds to detecting local maxima in this new domain. This transform is an evolution of that proposed in [8], which can be considered as an extension of the Hough Transform that operates with non-binary valued signals.

Let $F(t_n, d_k) = F[n, k]$ be the differential phase of a certain $N x K$ processing block in which segment detection is to be applied, where t_n represents the time instants within the

block time interval, and d_k the spatial positions along the optical fiber, with $1 \leq n \leq N$ and $1 \leq k \leq K$ the corresponding temporal and spatial samples. The first step is to compute the transform $M(r_i, s_j) = M[i, j]$ of the processing block at each point of the transformed domain. This computation essentially consists of calculating the median of the set of sample values of the block $F(t_n, d_k)$ within a certain straight segment defined by the parameters of the transformed domain (r_i, s_j), where r_i is the starting spatial position of the segment at the block's starting time; and s_j is the ending position of the segment at the block's ending time. Hence, the segment in the signal domain comprises a set of time-space tuples (t_n, d_n), where times are given by the sampling instants t_n and spatial positions are computed as:

$$d_n = r_i + \frac{s_j - r_i}{\Delta t} t_n \tag{1}$$

In order to adapt it to a discretized spatial domain, a rounding operation can be applied over the segment positions d_n so that each of them exactly corresponds to a certain sampling position of the signal d_k. Thus, $d_n \leftarrow d_k$ such that it minimizes $|d_n - d_k|$. The median signal values within the segment, i.e., the transform value at (r_i, s_j) is given by

$$M(r_i, s_j) = \text{median}\left[\{F(t_n, d_n)\}_{n=1}^N \right] \tag{2}$$

The sampling resolution of the transformed axes r_i and s_j is set to 1.8 m. An additional restriction is imposed to the points of the transformed domain to be computed: only those points for which the segment represents a moving velocity in the range [2, 60] m/s are computed.

Once the transformed map $M(r_i, s_j) = M[i, j]$ is obtained, local maxima of the map are extracted. Note that the locations of these maxima correspond to segments of the signal in which the median amplitude value is higher, implying a high probability that these segments correspond to the passage of a moving vehicle. Therefore, after computing a segment detection stage for a certain processing block, a set of local maxima in the transformed domain $\{(r_l, s_l)\}_{l=1}^L$ is available (marked with colored crosses in Figure 3 (d)), where l indexes the different detected and validated locations. These points correspond to specific straight segments in the non-transformed domain considered as potential moving vehicles, as shown in Figure 3 (e), where the colors of each trajectory correspond to those of the local maxima in Figure 3 (d).

Once local segments are detected at each processing block, the next step is to join these segments among the different blocks so that arbitrarily large trajectories corresponding to detected moving vehicles are obtained. The input of the tracking algorithm is the set of local maximum points in the transformed domain $\{p_l^m\}_{l=1}^{L_m} = \{(r_l^m, s_l^m)\}_{l=1}^{L_m}$ detected at each processing block, where m indexes the different processing blocks, with L_m the number of points of the mth block. The proposed tracking algorithm dynamically initiates, expands and ends trajectories as the sets of points of new blocks are being considered. Trajectories are defined as sequences of points in the transformed domain, where each point belongs to a different processing block. In this way, the qth trajectory is denoted as $\left\{w_q^m\right\}_{m=m_{\text{ini}q}}^{m_{\text{end}q}} = \left\{\left(r_{w_q}^m, s_{w_q}^m\right)\right\}_{m=m_{\text{ini}q}}^{m_{\text{end}q}}$, where $m_{\text{ini}q}$ and $m_{\text{end}q}$ are the indexes of the processing blocks in which the trajectory begins and ends; and $\left(r_{w_q}^m, s_{w_q}^m\right)$ is the point location in the transformed domain for the trajectory q in the block m.

Each point of the first processing block gives rise to the generation of a new trajectory, which is initialized containing only the point under consideration. In an iterative procedure, the points of new processing blocks are joined to the already existing trajectories by means of a distance criterion. This process also enables the generation of new trajectories, as well as the termination of existing ones, which is a key feature in a real-field environment. Next, for each processing block, the distance between the point of each provisional trajectory q in the mth processing block (the current endpoint of the trajectory), and each point l detected in the $m + 1$th processing block is calculated

$$\text{dist}\left[w_q^m, p_l^{m+1}\right] = \sqrt{D_r{}^2 + D_s{}^2} \tag{3}$$

where

$$D_r = \left(r_{wq}^m - r_l^{m+1}\right) + \frac{\delta t}{2\Delta t}\left(s_{wq}^m - r_{wq}^m + s_l^{m+1} - r_l^{m+1}\right) \tag{4}$$

$$D_s = \left(s_{wq}^m - s_l^{m+1}\right) + \frac{\delta t}{2\Delta t}\left(s_{wq}^m - r_{wq}^m + s_l^{m+1} - r_l^{m+1}\right) \tag{5}$$

Points of block $m + 1$ are joined to the provisional trajectories in an iterative process, in which, at each iteration, the combination w_q^m, p_l^{m+1} with the lowest distance gives rise to a new union. This process ends when there is no joint whose distance is less than the maximum allowed distance. Once a trajectory is closed, if its length is shorter than a certain number of points, the trajectory is discarded. Otherwise, it is incorporated to the set of definitive trajectories. Finally, a last step is applied to describe these trajectories as a sequence of time-distance tuples in the non-transformed domain. In this domain each trajectory actually represents a sequence of segments among the different processing blocks. Therefore, the time and position in the middle of the segment is chosen as the time-distance coordinate of the trajectory within the segment. Figure 3 (b) represents these trajectories, as colored points superimposed to the grey-scale map of the signal in Figure 3 (a), showing excellent results.

4. Classification

The output of the tracking algorithm is a set of trajectories each of which can be regarded as a vehicle passing event. The next stage in the processing system aims to classify the vehicle passing events according to its size (cars (C) and trucks (T)) and travel direction (go (G) and return (R)), leading to four different classes: CG, CR, TG, and TR. In order to enhance the classification ability of the system, three additional classes have been defined: motorbikes travelling in each direction (MG and MR) and a not-a-vehicle class (NV), comprising all the spurious trajectories coming from the tracking algorithm but not related to any real vehicle passing event. Hence, the classification system was designed to be able to identify among seven different vehicle passing event classes. Before proceeding with the feature extraction from the signals, a vehicle signature signal was extracted from each trajectory. The vehicle signature signal (Figure 4(a-b)) is a two-dimensional signal extracted from the phase signal limiting the slow-axis extent to a +-2 s interval around the trajectory for each of the fast-axis traces. From this signal, the vehicle signature trace (Figure 4(c)) was calculated by taking the median of the vehicle signature signal in the fast-axis dimension, hence obtaining a one-dimensional signal that varies in the slow-axis. This can be regarded as an averaged signal representing the impact of a vehicle when passing across an average point of the road.

In the left row of Figure 5, the vehicle signature traces aggregated by its corresponding class are depicted. In the right row of Figure 5, the median from all the signature trace for each class, along with the 25th and 75th percentile limits are depicted. It is important to observe that, in general terms, the signal amplitude of the signature traces corresponding to the motorcycle class is lower than that corresponding to the car class, and in turn, the amplitude for the car class is notably lower than that corresponding to the truck class. Furthermore, the amplitude is generally larger for the traces corresponding to the go direction than for those corresponding to the return direction. This is due to the fact that the fiber is placed on the shoulder next to the go direction lane, resulting in a higher sensitivity for the vehicles moving in that direction. Regarding the class of non-vehicles, it is observed that a great amount of the signal activity tends to appear on the sides of the interval analysis, especially in the negative time side, something that is not observed for the rest of the classes. It is also observed that only in the non-vehicle class there are signature traces whose value in the center of the interval analysis is negative.
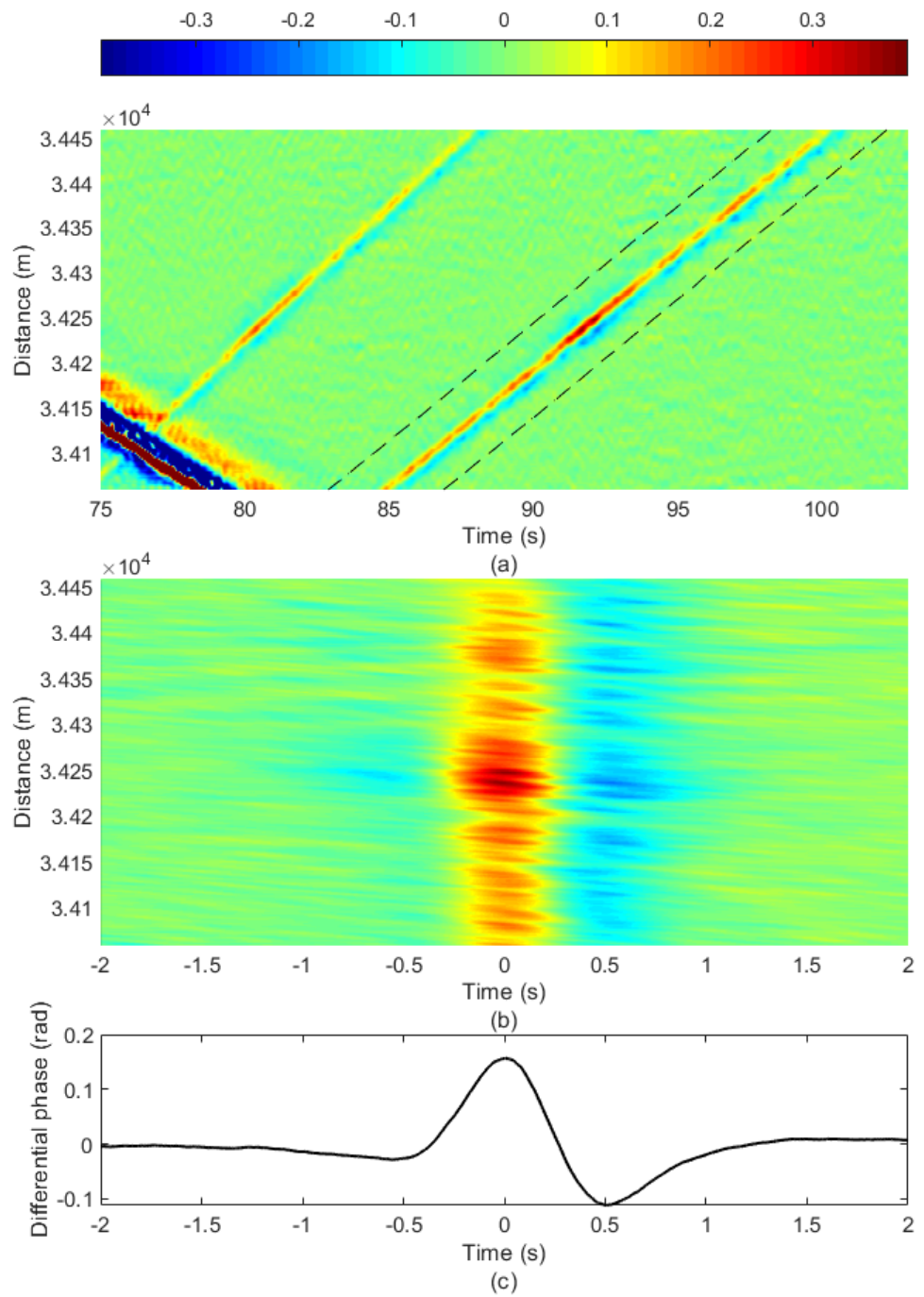
Figure 4. Vehicle passing event represented by: (**a**) the vehicle signature signal, (**b**) a two-dimensional crop of the optical phase signal of +-2 s around the trajectory; and (**c**) the vehicle signature trace, an averaged version of the former signal to summarize the vehicle signature in the slow-axis.

In agreement with the previously described behavior, feature extraction was designed to extract relevant information from the differences among the vehicle signature traces of the different classes observed in Figure 5. Four features are extracted from the vehicle signature traces:

- Peak-to-peak amplitude: calculated as the decimal logarithm of the peak to peak amplitude of the signature trace restricting the analysis to 1 s of the signal around its center (in Figure 5, within the interval delimited by dashed red lines).
- Center amplitude: calculated as the amplitude of the signature trace in its central sample.
- Lateral area: calculated as the decimal logarithm of the summated absolute amplitude values of the signature trace after removing the 1 s central part of the signal.
- Velocity: calculated directly from the trajectory, as the total signed travel of the trajectory in the fast-axis, divided by its time span in the slow-axis.

Figure 6 presents the two-dimensional scatter plot projections of the four-dimensional feature space. Peak-to-peak amplitude is closely related to the vehicle weight: the greater the weight, the greater the amplitude. For this reason, this feature is useful to separate between the car classes (CR and CG), and the truck classes (TR and TG). However, this feature is less useful to separate between the motorcycle classes (MR and MG) and the car classes (CR and CG) (HABRIA QUE MATIZAR ESTA AFIRMACION, EXPLICANDOLO MEJOR). The center amplitude is also related to the vehicle weight, providing a similar behavior in terms of separability between classes. However, it is convinient to add this feature to the classification stage, as it provides additional information when separating the non-vehicle class from the rest of the classes. Note that this class is the only one for which several signature traces present a negative value in the center of the interval. Therefore, it provides an straightforward way to separate those negative amplitude cases in the non-vehicle class. Regarding the lateral area, which measures the signal activity on the sides of the window, it clearly provides separability in the non-vehicle class. It must be taken into account that many of the spurious trajectories detected by the segmentation algorithm (labeled as non-vehicles) are originated as a consequence of the passage of a truck, which systematically produces a positive after-wave that is detected as a spurious trajectory in the segmentation. This is the reason why the non-vehicle class, systematically presents a lot of signal activity on one side of the window. Regarding the velocity, its sign allows a clear separation between classes corresponding to the go direction (negative velocity), and those corresponding to the return direction (positive velocity).

A set of 512 labelled feature vectors was employed to train and evaluate an SVM classifier within the Matlab Classification Learner App. Evaluation was performed under a five-fold cross-validation scheme with 80% of the observations dedicated to training and 20% of the observations dedicated to test.

Classification results are shown in the confusion matrix of Figure 7. Results show a high classification accuracy of 98.8% for the vehicle passing events. When analysing the confusion matrix, it is important to note that 56 out of 57 not-a-vehicle events are correctly classified. These are spurious trajectory detections left by the tracking algorithm that our classifier is able to detect and tag to be removed from further analysis. As a consequence, the classification stage is able to further refine the results from the trajectory tracking algorithm, implementing a second check on its results. In the same vein, incorporating the motorbike classes (in both directions), helps reducing the number of misclassified car and truck trajectories, as the classifier is able to identify these events as vehicles but not in the car or truck classes. Of the 27 truck events analyzed keeping in mind the two road directions, 24 have been correctly classified, and 3 have been wrongly classified as cars. The erroneous cases correspond to very light trucks, for which the amplitude of the signature trace is small compared to that corresponding to an average truck signature. Regarding the car events, of the total of 453 cases analyzed, 452 have been correctly classified (99.8%), and only one has been misclassified, specifically as a truck. The reason for this misclassification is most likely due to the fact that the car had a significantly higher weight than the average car, which means that its signature amplitude is also higher than the average car signature. Another aspect to take into account is that in no case has a vehicle in one direction of the road been classified as a vehicle in the other direction.
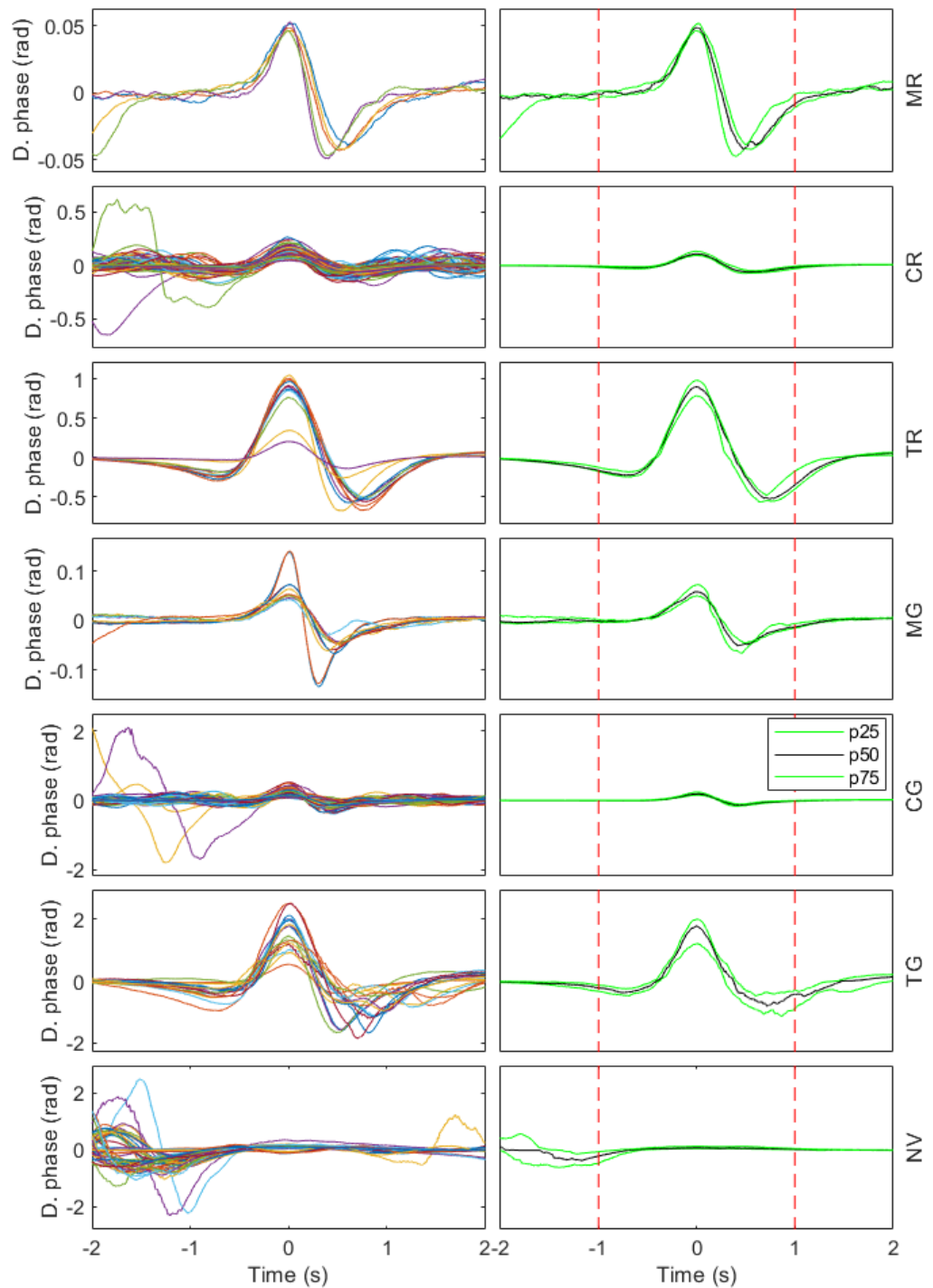
Figure 5. Vehicle signature traces of all the analyzed events grouped by class (left row) and the corresponding median trace and 25th and 75th percentile signals per class (right row). Each column corresponds to one of the analyzed classes: MR, CR, TR, MG, CG, TG and NV. The vertical dashed red lines in the lower row represent, at each plot, the time instants at -1 s and 1 s.

5. Discussion and conclusions

EXTENDER We have demonstrated a long-range and high-resolution automatic traffic monitoring scheme which takes advantage of the enhanced sensing capabilities provided by optical pulse compression in distributed phase-sensitive optical time-domain reflectometry.
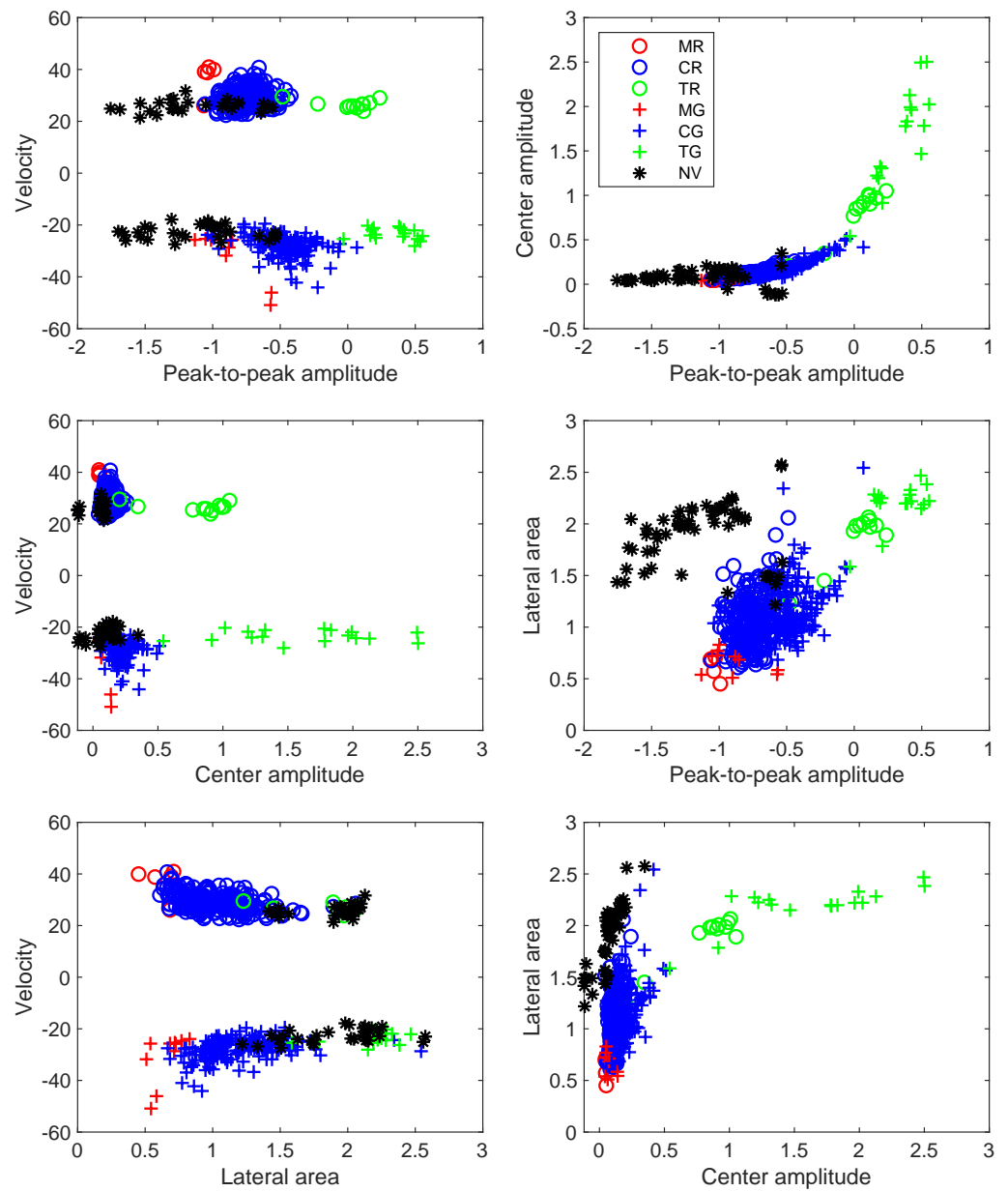
Figure 6. Two-dimensional scatter plot projections of the four-dimensional feature space showing the feature vectors of the seven classes: MR (red circles), CR (blue circles), TG (green circles), MR (red crosses), CR (blue crosses), TG (green crosses), and NV (black asterisks). The plots correspond to the feature combinations: peak-to-peak amplitude vs velocity; center amplitude vs velocity; lateral area vs velocity; peak-to-peak amplitude vs center amplitude; peak-to-peak amplitude vs lateral area; and center amplitude vs lateral area.

In addition, a vehicle detection and tracking algorithm has been developed, based on a novel transformed domain, enabling high-accuracy non-machine-learning-based traffic monitoring, which could be an advantage in certain scenarios as it does not require a training stage. Further work should focus on exploring the capabilities of the vehicle detection algorithm to provide vehicle classification or other valuable information for traffic management.

Figure 7. Confusion matrix showing the classification outcome for the different classes. The rows correspond to the true class, and the columns to the predicted class.

Abbreviations

The following abbreviations are used in this manuscript:

DAS   Distributed Acoustic Sensing
OPC   optical pulse compression
COTDR   coherent optical time-domain reflectometry
SNR   signal-to-noise ratio

References

1. AU Hubbard, Peter G. Xu, J.; Zhang, S.; Dejong, M.; Luo, L.; Soga, K.; Papa, C.; Zulberti, C.; Malara, D.; Fugazzotto, F.; Garcia Lopez, F.; et al. Dynamic structural health monitoring of a model wind turbine tower using distributed acoustic sensing (DAS). *Journal of Civil Structural Health Monitoring* **2021**, *11*, 833–849. https://doi.org/https://doi.org/10.1007/s13349-021-00483-y.
2. Wang, C.; Olson, M.; Sherman, B.; Dorjkhand, N.; Mehr, J.; Singh, S. Reliable Leak Detection in Pipelines Using Integrated DdTS Temperature and DAS Acoustic Fiber-Optic Sensor. In Proceedings of the 2018 International Carnahan Conference on Security Technology (ICCST), 2018, pp. 1–5. https://doi.org/10.1109/CCST.2018.8585687.
3. Gonzalez-Herraez, M.; Fernandez-Ruiz, M.R.; Magalhaes, R.; Costa, L.; Martins, H.F.; Becerril, C.; Martin-Lopez, S.; Williams, E.; Zhan, Z.; Vantilho, R. Distributed Acoustic Sensing for Seismic Monitoring. In Proceedings of the Optical Fiber Communication Conference (OFC) 2021. Optica Publishing Group, 2021, p. Tu1L.2. https://doi.org/10.1364/OFC.2021.Tu1L.2.
4. Peng, F.; Wu, H.; Jia, X.H.; Rao, Y.J.; Wang, Z.N.; Peng, Z.P. Ultra-long high-sensitivity Φ-OTDR for high spatial resolution intrusion detection of pipelines. *Opt. Express* **2014**, *22*, 13804–13810. https://doi.org/10.1364/OE.22.013804.
5. Wiesmeyr, C.; Litzenberger, M.; Waser, M.; Papp, A.; Garn, H.; Neunteufel, G.; Döller, H. Real-Time Train Tracking from Distributed Acoustic Sensing Data. *Applied Sciences* **2020**, *10*. https://doi.org/10.3390/app10020448.
6. Wang, H.F.; Fratta, D.; Lancelle, C.; Ak, E.M.; Lord, N.E. Distributed Acoustic Sensing (DAS) Array near a Highway for Traffic Monitoring and Near-Surface Shear-Wave Velocity Profiles. In Proceedings of the AGU Fall Meeting Abstracts, 2017, Vol. 2017, pp. S33B–0866.

7.   Huang, M.F.; Salemi, M.; Chen, Y.; Zhao, J.; Xia, T.J.; Wellbrock, G.A.; Huang, Y.K.; Milione, G.; Ip, E.; Ji, P.; et al. First Field Trial of Distributed Fiber Optical Sensing and High-Speed Communication Over an Operational Telecom Network. *Journal of Lightwave Technology* **2020**, *38*, 75–81. https://doi.org/10.1109/JLT.2019.2935422.

8.   Chambers, K. Using DAS to investigate traffic patterns at Brady Hot Springs, Nevada, USA. *The Leading Edge* **2020**, p. 819–827. https://doi.org/10.1190/tle39110819.1.

9.   Catalano, E.; Coscetta, A.; Cerri, E.; Cennamo, N.; Zeni, L.; Minardo, A. Automatic traffic monitoring by φ-OTDR data and Hough transform in a real-field environment. *Appl. Opt.* **2021**, *60*, 3579–3584. https://doi.org/10.1364/AO.422385.

10. Bao, X.; Zhou, D.P.; Baker, C.; Chen, L. Recent Development in the Distributed Fiber Optic Acoustic and Ultrasonic Detection. *Journal of Lightwave Technology* **2017**, *35*, 3256–3267. https://doi.org/10.1109/JLT.2016.2612060.

11. Martins, H.F.; Martin-Lopez, S.; Corredera, P.; Ania-Castañon, J.D.; Frazão, O.; Gonzalez-Herraez, M. Distributed Vibration Sensing Over 125 km With Enhanced SNR Using Phi-OTDR Over a URFL Cavity. *Journal of Lightwave Technology* **2015**, *33*, 2628–2632. https://doi.org/10.1109/JLT.2015.2396359.

12. Chen, D.; Liu, Q.; He, Z. 108-km Distributed Acoustic Sensor With 220-pε/$\sqrt{\text{Hz}}$ Strain Resolution and 5-m Spatial Resolution. *Journal of Lightwave Technology* **2019**, *37*, 4462–4468. https://doi.org/10.1109/JLT.2019.2901276.

13. Zhang, J.; Wu, H.; Zheng, H.; Huang, J.; Yin, G.; Zhu, T.; Qiu, F.; Huang, X.; Qu, D.; Bai, Y. 80 km Fading Free Phase-Sensitive Reflectometry Based on Multi-Carrier NLFM Pulse Without Distributed Amplification. *Journal of Lightwave Technology* **2019**, *37*, 4748–4754. https://doi.org/10.1109/JLT.2019.2919671.

14. Waagaard, O.H.; Rønnekleiv, E.; Haukanes, A.; Stabo-Eeg, F.; Thingbø, D.; Forbord, S.; Aasen, S.E.; Brenne, J.K. Real-time low noise distributed acoustic sensing in 171 km low loss fiber. *OSA Continuum* **2021**, *4*, 688–701. https://doi.org/10.1364/OSAC.408761.

15. Zou, W.; Yang, S.; Long, X.; Chen, J. Optical pulse compression reflectometry: proposal and proof-of-concept experiment. *Opt. Express* **2015**, *23*, 512–522. https://doi.org/10.1364/OE.23.000512.

16. Wang, S.; Fan, X.; Liu, Q.; He, Z. Distributed fiber-optic vibration sensing based on phase extraction from time-gated digital OFDR. *Opt. Express* **2015**, *23*, 33301–33309. https://doi.org/10.1364/OE.23.033301.

17. Wang, S.; Zou, W.; Long, X.; Chen, J. Influence of phase noise on measurement range in optical pulse compression reflectometry. In Proceedings of the 2015 Opto-Electronics and Communications Conference (OECC), 2015, pp. 1–3. https://doi.org/10.1109/OECC.2015.7340220.

18. Awwad, E.; Dorize, C.; Guerrier, S.; Renaudier, J. Detection-Localization-Identification of Vibrations Over Long Distance SSMF With Coherent $\Delta\phi$-OTDR. *Journal of Lightwave Technology* **2020**, *38*, 3089–3095. https://doi.org/10.1109/JLT.2020.2993167.

19. Loayssa, A.; Sagues, M.; Eyal, A. Phase noise effects on phase-sensitive OTDR sensors using optical pulse compression. *Journal of Lightwave Technology* **2021**, pp. 1–1. https://doi.org/10.1109/JLT.2021.3138249.

20. Chen, D.; Liu, Q.; He, Z. Phase-detection distributed fiber-optic vibration sensor without fading-noise based on time-gated digital OFDR. *Opt. Express* **2017**, *25*, 8315–8325. https://doi.org/10.1364/OE.25.008315.